10 | https://doi.org/10.3311/PPci.20593
Creative Commons Attribution

Periodica Polytechnica Civil Engineering, 67(1), pp. 10–23, 2023

Modeling of Ultra-high Performance Fiber Reinforced Concrete Filled Steel Tube Columns under Eccentric Loading

Mohammed Sakr[1], Bothaina Osama[1*]

[1] Department of Structural Engineering, Faculty of Engineering, Tanta University, El-Gaish Str., Tanta Qism 2, Tanta, Egypt
* Corresponding author, e-mail: bothina69544@f-eng.tanta.edu.eg

Received: 03 June 2022, Accepted: 11 September 2022, Published online: 20 September 2022

Abstract

Recently, ultra-high performance fiber reinforced concrete (UHPFRC) has been commonly used as a structural material. In this study, finite element (FE) model is constructed to investigate the behavior of ultra-high performance fiber reinforced concrete filled steel tube columns (UHPFRCFSTs) under axial or eccentric loading. The analysis included three-dimensional FE model using solid elements. The novelty of the suggested FE model is the consideration of the confinement of the UHPFRC in-filled material. Furthermore addition, the numerical model includes initial local and overall geometric imperfections, as well as the inelastic response of both UHPFRC and steel materials. The interaction between the steel tube and UHPFRC in-filled is modelled using surface to surface contact. Experimental results from the literature are used to validate the FE model. It is proved that the FE model can predict the ultimate capacities, failure modes, and post-cracking behavior accurately for both short and long UHPFRCFSTs. The FE interaction diagram agreed very well with the experimental results. Using the verified FE model, a parametric study on UHPFRCFSTs is carried out. Several parameters, including concrete strength material, steel yield strength, and aspect ratio of the columns (column diameter/tube thickness), are investigated. Eventually, comparisons are conducted between the results obtained from FE simulation and the existing design codes for predicting load-moment interaction diagram of UHPFRCFSTs. It has been found that the Eurocode 4 predictions in most analyzed cases are conservative for UHPFRCFSTs.

Keywords

finite element model, composite columns, interaction diagram, UHPFRC

1 Introduction

Composite members made from a mix of steel and concrete enjoy the merits of both materials [1], specifically the high ductility and tensile strength of steel, the high compressive strength of concrete and its capability to stop the local buckling of steel tube. Additionally, the steel tube provides confinement mechanism for the concrete. Composite columns have become increasingly popular in a variety of engineering constructions, particularly high-rise buildings and long-span bridges [2]. The most common steel–concrete composite member is the concrete filled steel tube (CFST) column. The structural performance of CFST members has been the subject of numerous experimental and analytical research [3–5]. Relevant design specifications have been established in various nations and areas as a result of these findings to better guide the design of CFST members and structures.

To fulfil the ever-increasing performance demands of engineered constructions, high performance materials for instance high strength concrete (HSC) and fiber reinforced concrete (FRC) have gradually evolved into appealing alternatives to normal concrete in CFST members because of advanced material technologies. The use of HSC is thought to increase the risk of brittle failure of members, which can be avoided by utilizing steel tubes with a small diameter-to-thickness ratio [6].

It is an effective approach to improve the brittleness of the concrete core by inserting steel fibers to enable ductile behavior for such CFST members. Steel fibers were found to improve not only load-bearing capacity but also stiffness, delaying lateral deflection and boosting ductility and energy absorption capability of CFST members [7–8]. Ultra-high performance fiber reinforced concrete (UHPFRC) is a new

Cite this article as: Sakr, M., Osama, B. "Modeling of Ultra-high Performance Fiber Reinforced Concrete Filled Steel Tube Columns under Eccentric Loading", Periodica Polytechnica Civil Engineering, 67(1), pp. 10–23, 2023. https://doi.org/10.3311/PPci.20593

type of concrete material with better features in terms of compressive and tensile strength, as well as durability. It is characterized by ultra-high strength, good fracture toughness, and increased ductility [9–14]. Super-plasticizers are used to achieve great workability and self-compacting qualities despite a low water-cement ratio and provision of fiber. Several scholarships done on both its durability, overall performance, and characteristics had thus far yielded positive outcomes [15–18].

Nevertheless, there are many scholars investigated the behavior of CFST columns [19–25], there are only a few published studies on the behavior of ultra-high performance fiber reinforced concrete filled steel tube columns (UHPFRCFSTs) [26–30]. Mursi and Uy [19, 20] investigated the structural performance of rectangular CFST columns which were slender. According to their findings, the slender columns broke due to a combination of global instability and tube local buckling. When compared to their hollow equivalents, the filled concrete greatly boosted the capabilities of CFST columns. The strength and stiffness of CFST columns were significantly lowered when the eccentricity-to-width (e/B) ratio was increased. Sakino et al. [21] conducted an experimental study using 114 specimens to determine the impact of high-strength materials on the performance of short circular and rectangular CFST columns. The filled concrete's strength ranged from 25.4 to 85.1 MPa. The confinement in circular cross sections was more visible than in rectangular cross sections, according to the experiments. The strength of the composite columns was significantly increased by increasing either the steel yield stress or the concrete strength. The experimental performance of CFST rectangular columns fabricated by high-strength materials was explored by Huang et al. [22]. Steel plates were cut into the necessary forms and welded together to create CFST columns with B/t ratios ranging from 18 to 68. The rectangular steel boxes with significant B/t ratios experienced local buckling. Furthermore, raising the B/t ratio significantly lowered the capacity and stiffness of CFST columns. Through a combination of experimental and numerical research, Zhang et al. [23] studied the compressive behavior of steel reinforced concrete filled tubular (SRCFT) stub columns. The SRCFT stub columns displayed improved ductility than CFT stub columns. Shear cracks in the core concrete can be efficiently prevented by using the inserted steel section. Ding et al. [24] investigated the effect of orthogonal tension bars in rectangular CFST specimens with a high B/D ratio (from 1.0 to 3.0). The tension bars were shown to successfully limit tube lateral deformation and improve confinement on the infilled concrete, according to the findings. As a result, when tension bars are used, both ultimate strength and ductility increased significantly.

Xiong et al. [25] investigated the behavior of (CFSTs) with high and ultra-high strength materials at ambient temperature in an experimental research. The authors presented some new findings on the axial performance of 56 short CFSTs. Chen et al. [26] used an experimental investigation to investigate the structural behavior of UHPC-filled steel tube columns under axial loading. The primary goal of this research was to determine the mechanical differences between UHPCFST and CFST columns. The steel tube and UHPC performed well together in the tests, although the steel tube's augmentation effect on the core UHPC strength was not as great as that of normal concrete. Zhang et al. [27] experimentally investigated the behavior of UHPCFST columns subjected to eccentric loading. The findings revealed that when the initial eccentricity and slenderness ratio increased, the column's initial stiffness and load bearing capability dropped, and bending characteristics progressively emerged. Under eccentric compression, in-plane bending was the most common failure mode for UHPCFST columns. Yan et al. [28] investigated the axial behavior of square UHPFCFST columns experimentally. By varying the steel tube thickness and UHPC strength, the confinement index was used as a variable. All specimens showed good ductility, with confinement indexes ranging from 1.41 to 5.27. Hoang et al. [29] experimentally investigated the structural performance of UHPC and UHPC with steel fiber (UHPFRC) columns with steel tube. Axial loading was applied to all specimens. The results of the tests showed that loading only the concrete core resulted in a significant increase in strength and ductility. Shear plane failure of the UHPC and UHPFRC cores was observed in all specimens, which is often associated with softening behavior. An experimental research on the axial performance of square/rectangular UHPFRCFST columns was given by Yang et al. [30]. The ultimate axial stress of CFST columns was raised by increasing the thickness of the steel tube and adding steel fibers to the concrete mixture, according to the findings.

Although there are many scholars investigated the behavior of CFST columns numerically [31–33], there are limited published studies on UHPFRCFSTs. Hassanein and Patel [31] investigated the behavior of round-ended rectangular CFST (RRCFST) columns. The ABAQUS program was used to create three-dimensional finite element

(FE) models for RRCFST columns. The FE results agreed very well with previous experimental data. Ouyang and Kwan [32] analyzed the square concrete-filled steel tube (CFST) columns under axial compressive load using FE modeling. Overall, the full-range load-strain curves produced by the FE analysis were in good agreement with the experimental results. dos Santos et al. [33] reported on a study of the structural behavior of bolted shear connectors utilized as force transmission devices in concrete-filled composite columns using numerical modelling.

To the authors' knowledge, most existing studies have studied experimentally the behavior of UHPFRCFSTs under axial loading, with only a few numerical analyses reported, and neglecting the confinement of UHPFRC. To fill this numerical gap, a study investigating the behavior of UHPFRCFSTs under axial or eccentric loading conditions is required. The novelty of this finite element (FE) model was the consideration of the confinement in the UHPFRCFSTs. The research work presented in this paper discusses the eccentric behavior of UHPFRCFSTs and presents a FE model can predict the interaction diagram curve numerically. To accomplish this goal, finite element models are established using (ABAQUS) software [34] to mimic the behaviors of UHPFRCFSTs under axial or eccentric loading conditions. The FE model is then calibrated against experimental results published in previous studies [27].

2 Finite element models

ABAQUS software [34] is employed to mimic the behaviors of short and long UHPFRC filled steel tubular columns (UHPFRCFSTs) under both axial and eccentric loading. Detailed three-dimensional (3D) are conducted to predict their behavior. The constitutive models that are employed in the model are described briefly below. Load control method is implemented to estimate the column capacity and post-cracking behavior of the (UHPFRCFSTs).

2.1 Material properties and constitutive models

The "concrete damage plasticity model" (CDP) is implemented to mimic the nonlinear behavior of the confined UHPFRC. The major two failure modes in this model are tensile cracking and compressive crushing. Naeimi and Moustafa [35] proposed a model to establish the stress–strain relationships of confined UHPFRC materials. Their study shown that steel fiber had contributory roles in confining effects. Three different equations in three stages could be used to describe the limited compressive curve numerically (Fig. 1). The first region is a nonlinear

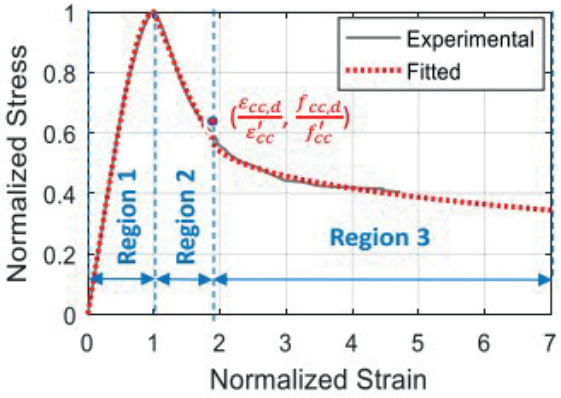

Fig. 1 Normalized compressive stress- strain curve for confined UHPFRC [35]

ascending branch from the origin up to peak strength. The second region is a nonlinear descending branch from the peak point to deteriorated strength at strain $\varepsilon_{cc,d}$. The third region is another nonlinear descending branch beyond $\varepsilon_{cc,d}$. The confined compressive stress-strain relationship of UHPFRC for three regions can be defined using these equations as follows:

$$f_c = \bar{f}_{cc}\left[\frac{2_1\left(\frac{\varepsilon_c}{\varepsilon_{cc'}}\right)^2}{2_1 - 1 + \left(\frac{\varepsilon_c}{\varepsilon_{cc'}}\right)^{2_1}}\right] \quad for \frac{\varepsilon_c}{\varepsilon_{cc'}} \le 1, \tag{1}$$

$$f_c = \bar{f}_{cc}\left[\frac{2_2\frac{\varepsilon_c}{\varepsilon_{cc'}}}{2_2 - 1 + \left(\frac{\varepsilon_c}{\varepsilon_{cc'}}\right)^{2_3}}\right] \quad for\, 1 \le \frac{\varepsilon_c}{\varepsilon_{cc'}} \le x_d, \tag{2}$$

$$f_c = \eta_d \bar{f}_{cc}\left[e^{-k1\left(\frac{\varepsilon_c - \varepsilon_d}{\varepsilon_{cc'}}\right)^{k2}}\right] \quad for\, xd \le \frac{\varepsilon_c}{\varepsilon_{cc'}}. \tag{3}$$

Equation (1) is used to draw the first region of the curve where $\bar{f}_{cc}$ and $\varepsilon_{cc}{}'$ refer to the peak compressive stress and strain, B_1 is the material parameter which could be calculated using Eq. (4). It should be noted that B_1, as displayed in Eq. (4), needs a value for the modulus of elasticity (E_c) that has been calculated using Eq. (5). $\bar{f}_{cc}$ is calculated using Eq. (6).

$$B_1 = \left[\frac{1}{1 - \left(\frac{f_{cc'}}{E_c\varepsilon_{cc'}}\right)^{2_1}}\right] \tag{4}$$

$$E_c = 3400\sqrt{f_{cu}} + 1310 v_f \tag{5}$$

$$\bar{f}_{cc} = f_{cu} + 6.26 v_f + 6.57 \rho_s \tag{6}$$

Where f_{cu} is the compressive strength of the unconfined UHPFRC, v_f is the volumetric ratio of steel fiber, and ρ_s is the volumetric ratio of stirrups reinforcement. Equation (2) is used to draw the second region of the curve where B_2 and B_3 are the material parameters to be calculated using the suggested Eqs. (7) and (8), respectively.

$$B_2 = 3.096 - 0.0941 v_f - 0.2073 \rho_s \tag{7}$$

$$B_3 = 3.793 - 0.2314 v_f - 0..0100 \rho_s \tag{8}$$

As seen in Eq. (3), the third zone corresponds to residual strength, which is generated by the confining action of fibers and transverse reinforcement. Where η_d is defined before in Eq. (9), and k_1 and k_2 could be calculated using Eqs. (10) and (11) as follows:

$$\eta_d = 0.289 - 0.004 v_f - 0.052 \rho_s , \tag{9}$$

$$k_1 = 0.2392 - 0.0112 v_f - 0.0207 \rho_s , \tag{10}$$

$$k_2 = 0.8975 - 0.0613 v_f - 0.0129 \rho_s . \tag{11}$$

x_d, which is the normalized strain ($\frac{\varepsilon_{cc,d}}{\varepsilon_{cc'}}$) at post peak strain $\varepsilon_{cc,d}$ and could be calculated by Eq. (2) when f_c is taken equal to $\eta_d \bar{f}_{cc}$.

In this study (FE model), the tension stiffening is described as a uniaxial stress-cracking strain relationship. The uniaxial tensile behavior of UHPFRC is usually consists of three phases: linear elastic, strain hardening and strain softening phase. Because the fibers resist the opening of micro cracks by fiber bridging, and UHPFRC continues to take stress in the initial phase, stress is increased linearly without fracture formation until cracking strength is reached (elastic zone). The tension is increased again in the second phase with the creation of micro fractures as the fibers begin to pull away from the matrix until tensile strength is reached and the dispersion of small cracks is enlarged (strain hardening zone). In the third phase, isolated macro fractures form and propagate as the tensile strength is reached (strain softening zone). Finally, there is no more stress transfer through these isolated macro cracks, and the final fracture occurs [36]. According to AFGC-SETRA recommendations [37], Fig. 2 depicts the tensile laws for UHPFRC, which are separated into three phases: elastic, hardening, and softening. The tensile stresses at two different characteristic points (at $w_{0.3}$ and $w_{1\%}$) are stated as follows:

$$\sigma_{btu} = \frac{\sigma(W_{0.3})}{K \gamma_{bf}} , \tag{12}$$

$$\sigma_{u1\%} = \frac{\sigma(W_{1\%})}{K \gamma_{bf}} , \tag{13}$$

$$\varepsilon_e = \frac{f_{tj}}{E_{ij}} , \tag{14}$$

$$\varepsilon_{u0.3} = \frac{W_{0.3}}{l_c} + \frac{f_{tj}}{\gamma_{bf} E_{ij}} , \tag{15}$$

$$\varepsilon_{u1\%} = \frac{W_{1\%}}{l_c} + \frac{f_{tj}}{\gamma_{bf} E_{ij}} , \tag{16}$$

$$\varepsilon_{lim} = \frac{l_f}{4 l_c} , \tag{17}$$

where $w_{0.3}$ = crack width of 0.3 mm, $\varepsilon_{0.3}$ = strain at crack width equal to 0.3 mm, σ_{btu} = tensile stress at a crack width of 0.3 mm, $w_{1\%}$ = crack width corresponding to 0.01 H, ε_1 = strain corresponding to crack width at 0.01 H, $\sigma_{u1\%}$ = tensile stress corresponding to crack width at 0.01 H, and H being the column section length, γ_{bf} = partial safety factor, K = fiber orientation coefficient, f_{tj} = tensile strength within softening range, ε_e = elastic strain, E_{ij} = modulus of elasticity, l_f = fiber length, and l_c = characteristic length (usually ⅔ H).

As shown in Fig. 3, the steel tube is supposed to be an elastic-plastic material. In this investigation, the steel model proposed by Tao et al. [38] was used. This model is suitable for structural steel with a strength ranging from 200 MPa to 800 MPa. The yield strength (F_y), ultimate strength (F_u), and elastic modulus (E_s) are the only three factors required to determine the full range stress-strain curve, as shown in Fig. 3. A Poisson's ratio of 0.3 was adopted for the steel tube.

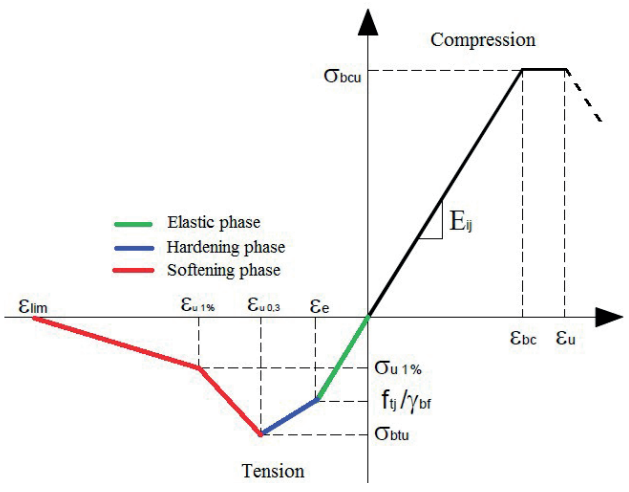

Fig. 2 Uniaxial stress-strain curve for UHPFRC [37]

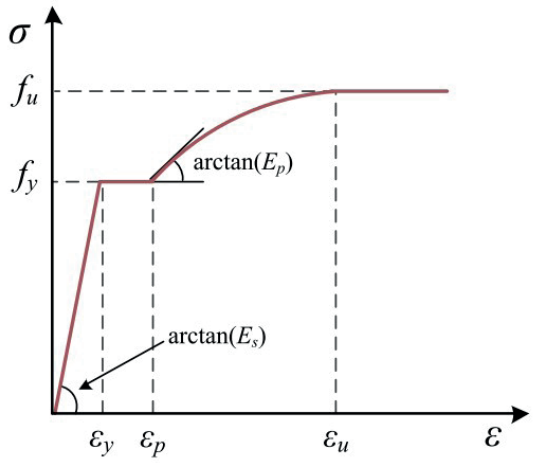

Fig. 3 Stress-strain model for steel tube proposed by Tao et al. [38]

2.2 Elements of the FE models

In this study, the behavior of UHPFRCFT columns is simulated using (ABAQUS). The analysis included solid element using 3D model. At 3D modeling using solid element, an 8-node 3-D solid element (C3D8R) is used for simulating the UHPFRC and steel tube.

2.3 Contact modelling

The interaction between the steel tube and the UHPFRC core was simulated by using surface-to-surface contact with a "hard" contact in the normal direction and a coulomb friction model (friction coefficient of 0.6) in the tangential direction. The interaction between the rigid loading plate and the UHPFRCFT columns was modelled by a tie contact interaction.

2.4 Equivalent geometric imperfection

The residual stresses for steel come from bending and initial geometric imperfection effects. Modeling the equivalent geometric imperfections necessitates choosing a suitable pattern for the geometric imperfections across the entire tube, as well as a suitable amplitude should be determined. To find the accurate imperfection pattern, an elastic buckling analysis was done for the UHPFRCFSTs and the accurate elastic buckling mode shape deformation was connected with the actual nonlinear FE model by using a simple subroutine obtainable in ABAQUS environment named IMPERFECTION. It is important to introduce these geometric imperfections with suitable out-of-plane deflection patterns and amplitudes into the nonlinear FE model to acquire accurate results. The amplitudes were considered for each model in this study as four levels (t_s, t_s/10, t_s/100, and L/1000) in order to evaluate the level that could provide satisfied FE predictions, where t_s, L are thickness of steel tube and length of the column, respectively.

3 Validation of the proposed FE model

Experimental data from prior work was utilized to validate the accuracy and applicability of the FE models of UHPFRCFST columns under eccentric loading. Zhang et al. [27] presented experimental results on six UHPFRCFST columns had a diameter of 108 mm circular cross section and 540 mm in height for short columns and 1080 mm in height for long columns. The short columns were tested under eccentric loading with eccentricities of 15, 30 mm, respectively. Moreover, the long columns were tested under eccentric loading with eccentricity of 15 mm. The UHPFRCFSTs columns had two thicknesses of steel tube of 4.24, 6.01 mm, respectively. Details of the tests are given in Table 1. The dimensions of test specimens are presented in Fig. 4.

Table 1 Detailed parameters of test specimens [27]

Specimens	D (mm)	t (mm)	L (mm)	F_y	F_c'	e
CS4-S-15	108.6	4.24	540	394.40	145.90	15
CS4-S-30	108.6	4.24	540	394.40	145.90	30
CS4-L-15	108.6	4.24	1080	394.40	145.90	15
CS6-S-15	108.1	6.01	540	420.90	145.90	15
CS6-S-30	108.1	6.01	540	420.90	145.90	30
CS6-L-15	108.1	6.01	1080	420.90	145.90	15

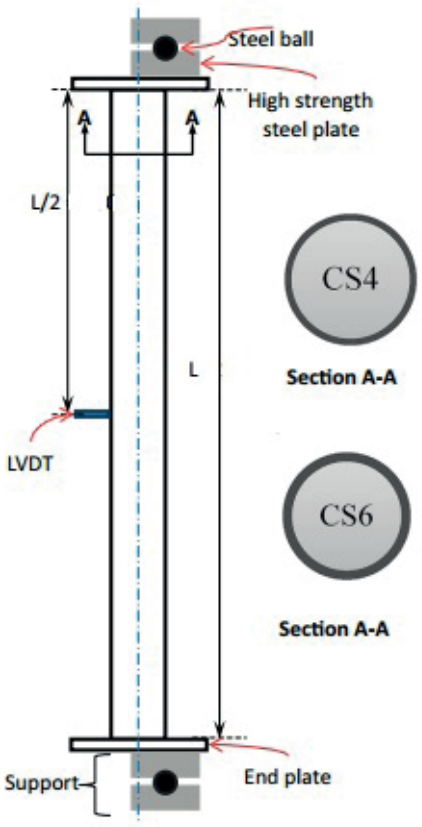

Fig. 4 The Dimensions details of test specimens [27]

3.1 Material properties in the FE models

The nonlinear behavior of UHPFRC material is divided into two regions: compression and tension. The proposed FE models of confined UHPFRC material in compression which calculated according to Eqs. (1)–(11), as displayed in Fig. 5(a). The tensile behavior of UHPFRC material was not provided in the experimental work, so the tension stiffening is extracted from a direct uniaxial test on dog bone specimens as displayed in Fig. 5(b) [27, 39]. The first cracking happened at a stress of, $f_{Ut,1}$ = 4.9 MPa, which typically corresponds to the cracking strength of the matrix. After cracking, the fibers struggled the tensile stresses by fiber bridging effect until the peak tensile strength is achieved. The production of micro-cracks throughout the specimen is caused by fiber bridging, and the material resists tensile pressures until the crack localizes. The average peak tensile strength of the material adopted in this study is, $f_{Ut,\max}$ = 5.8 MPa and the strain corresponding to the peak strength is, $\varepsilon_{Ut,\max}$ = 2800 micro-strain, while the softening stage starts and the stress fall rapidly due to the localization of the crack. The nonlinear behavior of steel tube material is displayed in Fig. 6 for two tube thicknesses.

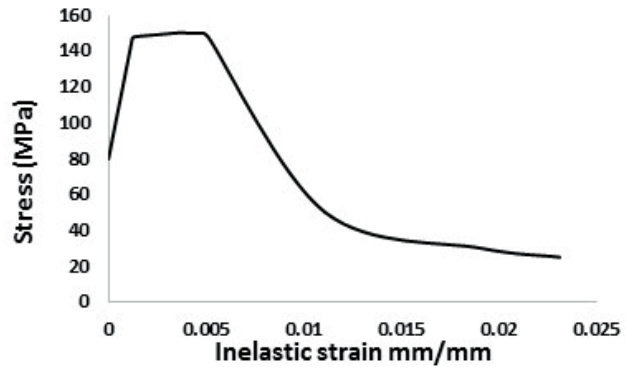

(a)

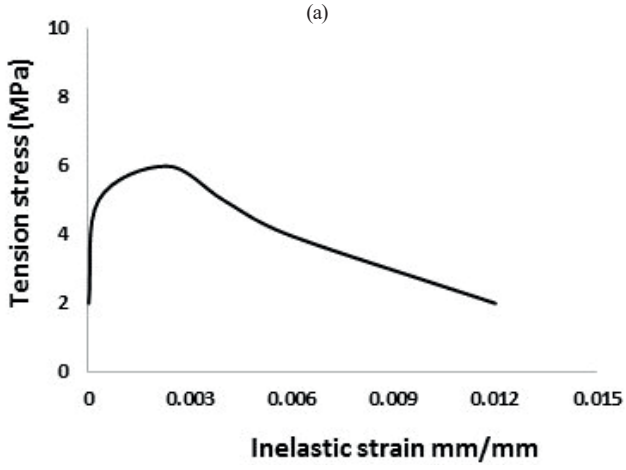

(b)

Fig. 5 Material properties of UHPFRC: (a) Compressive stress-strain responses for UHPFRC; (b) Tensile stress-strain responses for UHPFRC

3.2 Applied loads

In the experimental work, the columns were tested under eccentric loading. The test and FE models setup and loading system are displayed in Fig. 7. To mimic the experimental setup, rigid plates composited with a rectangular flat plate (length: 390 mm, width: 390 mm, thickness: 40 mm), were adopted, as presented in Fig. 7.

3.3 Imperfection sensitivity

The geometric imperfection value was taken as the column length over 1000 (*L*/1000) following Tao et al. [38].

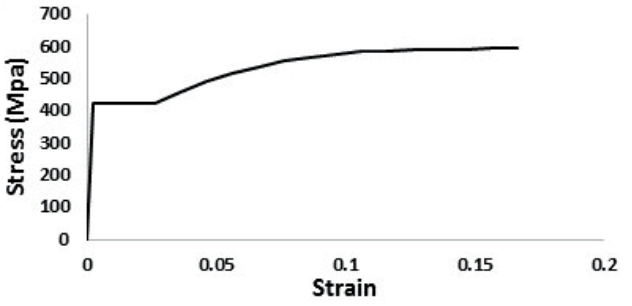

(a)

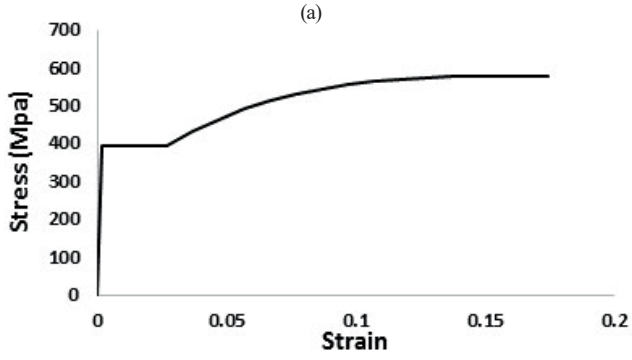

(b)

Fig. 6 Material properties of steel: (a) CS4; (b) CS6

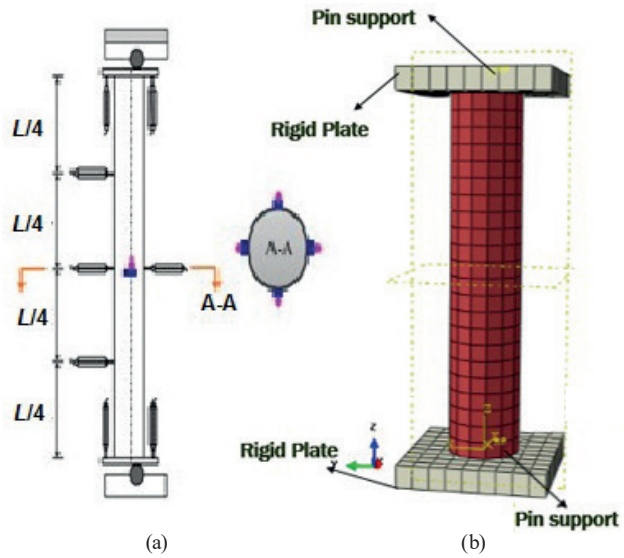

(a) (b)

Fig. 7 UHPFRCFSTs columns setup: (a) Experimental Zhang et al. [27]; (b) FE simulation (3D model)

Despite relating the imperfection to the length of the column as (L/1000) [38], the imperfection used in the current composite columns is still local in nature. Accordingly, additional values for the local geometric imperfection were also considered to confirm the final selected amplitude. Moreover, three values of 1, 10 and 100% of the steel tubular section column thickness (t_s) were examined as local imperfection amplitudes. Table 2 displays the ultimate FE load (N_{FE}) and the corresponding lateral displacement (Δu) of specimens CS4-S-15, CS4-L-15 for four utilized imperfection amplitude levels (t_s, t_s/10, t_s/100, and L/1000). From the comparison shown in Table 2 between the test and the FE results, the best match between the test results and the FE results was obtained when the amplitude of the geometric imperfection was L/1000. It can be observed in Table 2 that the ultimate load results are sensitive relative to the change in the geometric imperfection amplitudes. It was found that the displacement predictions are more sensitive to the change in the geometric imperfection amplitudes compared to the load predictions.

3.4 Mesh convergence

For determining a proper and stable mesh size, a mesh convergence study was done. Mesh convergence was studied in this work, which ranged from moderately coarse meshes to very fine meshes. The meshes element sizes are 100 mm, 80 mm, 40 mm, 20 mm, and 10 mm.

Table 2 Comparison of the test and FE key results for varying imperfection amplitude levels

	Imperfection amplitude level	Specimen label	
		CS4–S-15	CS4-L-15
N_{FE}	L/1000	1100	915
	ts	1096	900
	ts/10	1094	880
	ts/100	1089	850
Δ_{FE}	L/1000	5.70	10.50
	ts	5.30	10.00
	ts/10	5.10	9.50
	ts/100	4.90	8.90
N_{exp}/N_{FE}	L/1000	1.04	1.00
	ts	1.042	1.01
	ts/10	1.045	1.03
	ts/100	1.049	1.08
Δ_{exp}/Δ_{FE}	L/1000	1.10	1.00
	ts	1.19	1.05
	ts/10	1.24	1.15
	ts/100	1.29	1.17

Fig. 8(a) displays the results obtained for meshes with element sizes ranging from 120 mm to 10 mm for eccentrically loaded column (CS4-S-15). The results display that refinement of the mesh has little to no effect on the solution and increases CPU time as presented in Fig. 8(b). As a result, the 20 mm element meshes provide a satisfactory convergence.

3.5 Comparison of experimental and finite element results

Figs. 9(a)–(d) show the experimental and FE results of short UHPFRCFSTs columns subjected to load eccentricities of 15 (CS4-S-15, CS6-S-15), and 30 (CS4-S-30, CS6-S-30) mm. The load (kN) vs. mid height lateral displacement achieved for long UHPFRCFST columns from the experimental and FE analysis is presented in Figs. 10(a)–(b). From Fig. 9 and 10, the overall prediction is favorable, with only a minor variation in the descending stage. Moreover, the ultimate load capacities of the UHPFRCFSTs obtained from experimental data (N_{exp}) are compared with finite

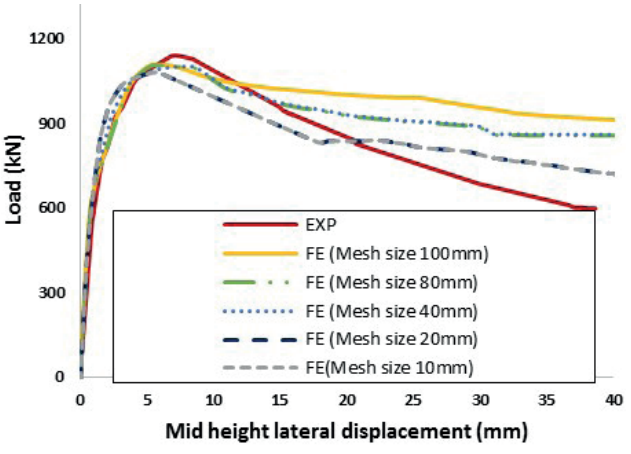

(a)

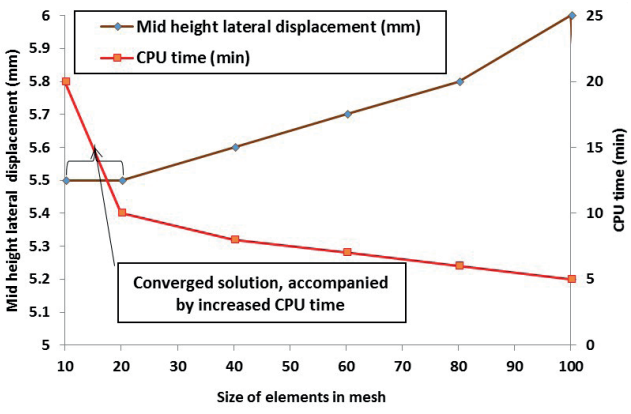

(b)

Fig. 8 Mesh convergence study for (CS4-S-15) specimen: Load vs. mid height lateral displacement; (b) Convergence vs. CPU time

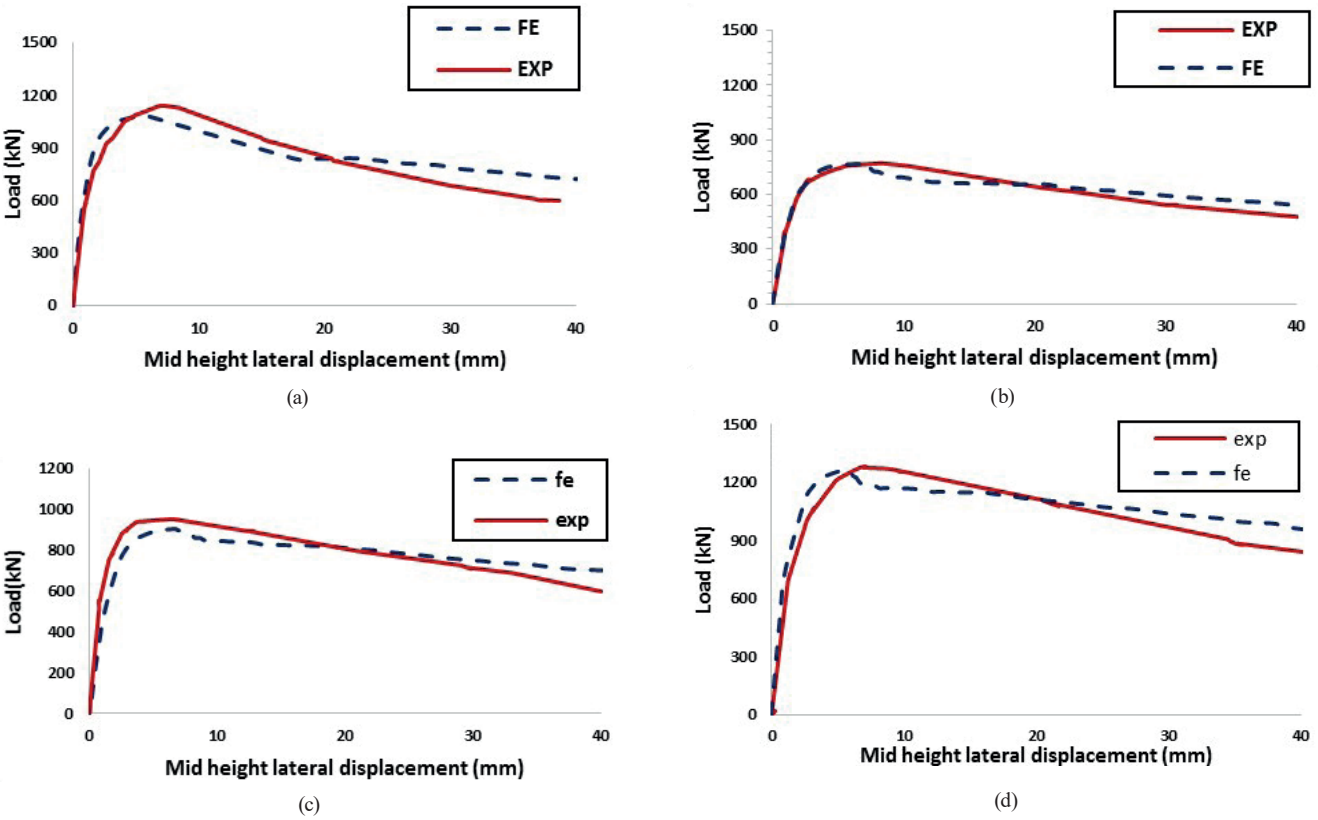

Fig. 9 Comparison of experimental results with (3D) FE model for short UHPFRCFSTs columns with different load eccentricities and thickness of steel tube: (a) CS4-S-15; (b) CS4-S-30; (c) CS6-S-15; (d) CS6-S-30

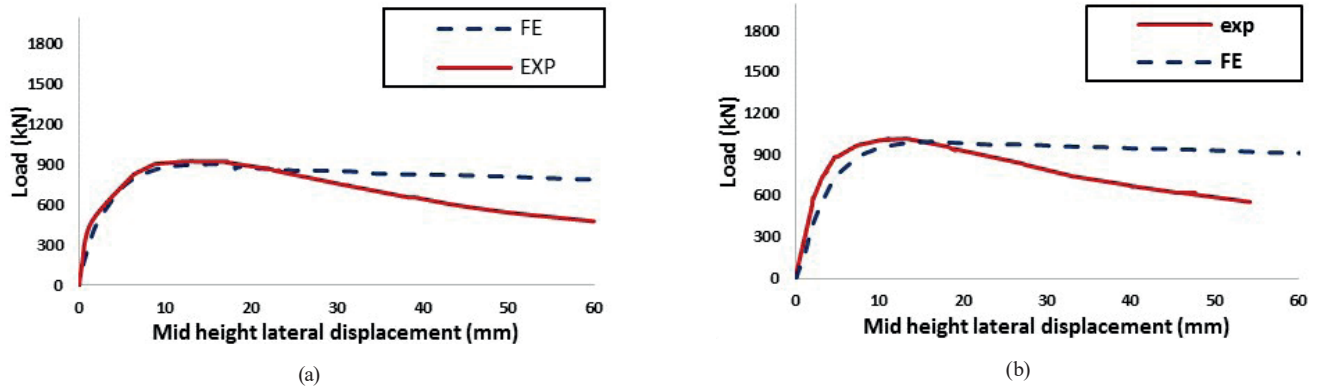

Fig. 10 Comparison of experimental results with (3D) FE model for long UHPFRCFSTs columns with different thickness of steel tube: (a) CS4-L-15; (b) CS6-L-15

element analyses (N_{FE}) in Table 3. The mean values of N_{FE}/N_{exp} and M_{FE}/M_{exp} are 0.96 and 0.99, and 0.91 and 1.03, respectively. Fig. 11 compares the deformation mode after failure between FE and test results. In terms of overall bending and local buckling, the FE model performed well. At the ultimate state, the compression and tension flanges at the mid-section of the steel tube have yielded, and the plastic distribution is decreasing towards both ends. Through the above verification and comparisons, it can be concluded that satisfactory agreement has been achieved between the FE simulation and the test results. This indicates that the currently established FE model can be used for further analysis of UHPFRCFST columns under eccentric compression.

4 Parametric study

The proposed FE model proved its ability to accurately represent the eccentric response of both short and long UHPFRCFSTs. The suggested verified FE model was adopted to investigate the effect of several parameters on the behavior of UHPFRCFST columns. These parameters

Table 3 Comparisons among of experimental, and FE results

Specimen label	Test [27]		FE			
	N_{exp} (kN)	M_{exp} (kN·m)	N_{FE} (kN)	N_{FE}/N_{exp}	M_{FE} (kN·m)	M_{FE}/M_{exp}
CS4–S-15	1143	25.40	1100	0.96	23.40	0.93
CS4–S-30	773	29.80	765	0.98	28.50	0.96
CS4-L-15	915	26.60	912	0.99	27.40	1.03
CS6–S-15	1284	28.40	1255	0.97	26.40	0.93
CS6–S-30	954	34.90	895	0.94	31.70	0.91
CS6–L-15	1016	28.70	985	0.96	26.50	0.92

include concrete strength material, steel yield strength, and aspect ratio of the columns (column diameter/tube thickness).

4.1 Concrete strength

To investigate the effects of concrete compressive strength, two more concrete compressive strengths were proposed in addition to that tested in the experimental work [27]. The effectiveness of the UHPFRC material is evaluated by comparing it with traditional solutions, based on the

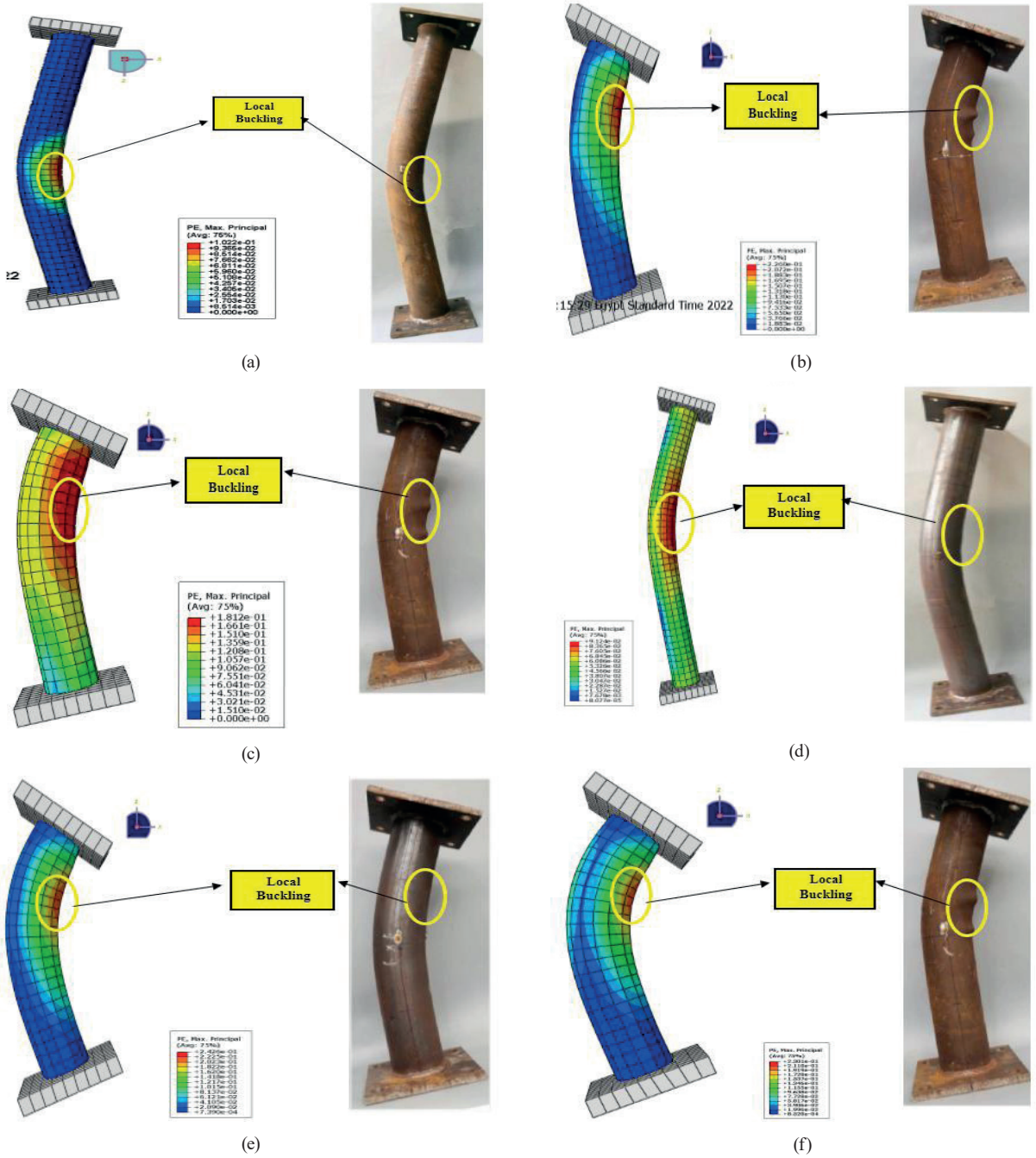

Fig. 11 Comparison between FE predicted and experimental failure modes: (a) CS4-L-15; (b) CS4-S-15; (c) CS4-S-30; (d) CS6-L-15; (e) CS6-S-15; (f) CS6S-30

adoption of normal strength concrete (NSC) and high strength concrete (HSC), to show how the UHPFRC has affected the response of the columns. The NSC and HSC columns have the same cross-section of columns [27]. The NSC column has compressive strength of 25 MPa and the HSC has compressive strength of 80 MPa. The steel yield strength of the steel tube was 394 MPa [27]. Fig. 12 shows the N-M interaction diagram curves of both short and long columns with different concrete strength materials and constant steel yield strength. It can be seen from this figure that the capacity of both short and long columns increased with the increase in the concrete compressive strength values. For example, UHPFRCFST short columns under pure axial loading showed almost 125% and 50% increase in axial load capacity compared to NSCFST and HSCFST columns, respectively. While, UHPFRCFST short columns under eccentric loading (CS4-S-30) showed almost 30% and 40% increase in load capacity compared to NSCFST and HSCFST columns, respectively. For UHPFRCFST long column under eccentric loading (CS4-L-30) showed almost 28% and 39% increase in load capacity compared to NSCFST and HSCFST columns. It should be noted that it is more efficient to use UHPFRC to increase the axial capacity rather than pure bending capacity as depicted in Fig. 12. The reasonable explanation for this is that the concrete exhibits a low tensile strength which reduces the pure bending capacity. The increase in concrete compressive strength did not make any changes in the failure mode of the simulated columns, which is local buckling followed by concrete crushing. It was found using UHPFRC material not only improves the load-bearing capacity but also improving the ductility of the columns.

4.2 Steel strength

Fig. 13 gives the *N–M* interaction diagram curves of both short and long columns (CS4) with varied steel strength, where the steel strengths are 235 MPa, 345 MPa, and

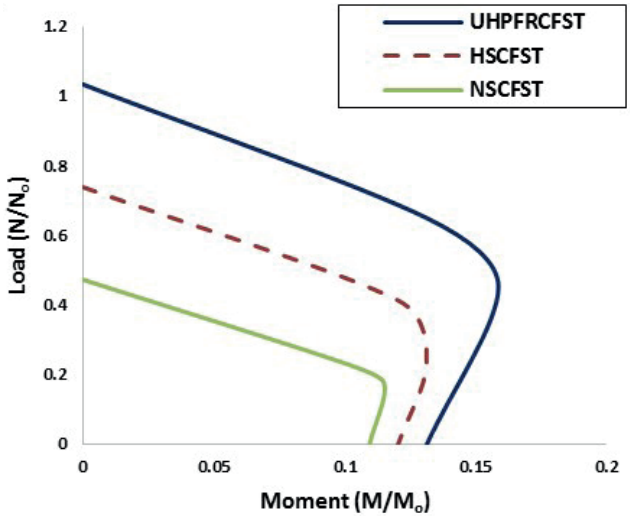

(a)

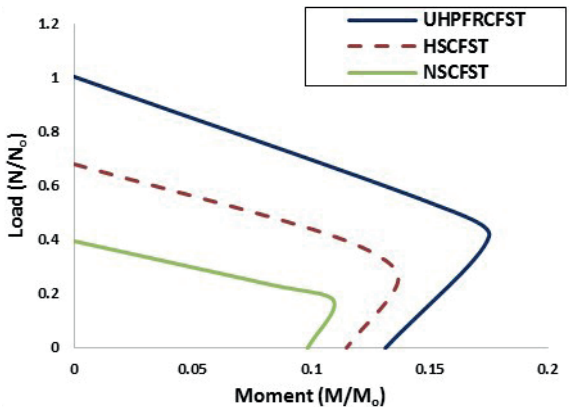

(b)

Fig. 12 *N–M* interaction diagram with different concrete material (F_y= 394 MPa): (a) short columns; (b) long columns

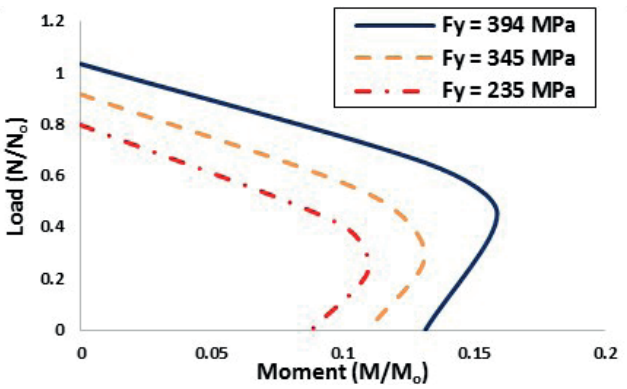

(a)

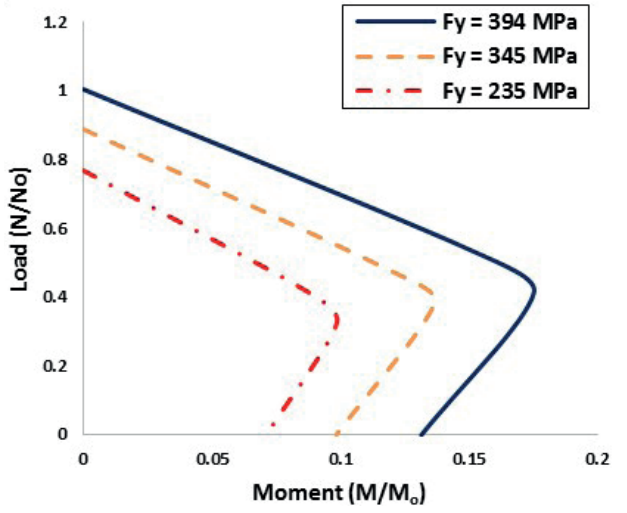

(b)

Fig. 13 *N–M* interaction diagram with different steel strength (UHPFRC material): (a) short columns; (b) long columns

394 MPa, respectively, while other parameters are kept the same (UHPFRC material). From Fig. 13, it can be found that the ultimate bearing capacities are improved by 17% (from 345 MPa to 394 MPa) and 38% (from 235 MPa to 345 MPa) with the increase of steel strength when both short and long columns subjected to pure axial loading. While, UHPFRCFST columns under eccentric loading (CS4-S-30), (CS4-L-30), it can be found that the ultimate bearing capacities are improved by 50% (from 345 MPa to 394 MPa) and 75% (from 235 MPa to 345 MPa) with the increase of steel strength. It indicates that it is more efficient to increase the steel strength to increase the pure bending capacity rather than the axial capacity as depicted in Fig. 13. This could be ascribed to the contribution of steel tube on carrying the tension load of the steel-concrete composite column under pure bending.

4.3 Column diameter/tube thickness (*D*/*t*)

In this section, the aspect ratio (diameter-to-thickness ratio) which is one of the factors that affect the fundamental behavior of UHPFRCFST columns is investigated. The *D*/*t* ratio is varied by choosing four different thicknesses comprising 3.00 mm, 4.20 mm, 6.00 mm, and 8.00 mm. Other properties such as yield strength of steel and compressive strength of concrete were maintained constant (394 MPa and 145 MPa, respectively). Fig. 14 gives the *N*–*M* interaction diagram curves of both short and long columns with varied *D*/*t* ratio. From Fig. 14, it can be found that the ultimate bearing capacities are improved by 25% from (25.60 to 36.20), 17% from (18.00 to 25.60), and 18% from (13.5 to 18.00) with the decrease of *D*/*t* ratio when both short and long columns subjected to pure axial loading. Moreover, when UHPFRCFST columns under pure bending, the bending capacity increases as the *D*/*t* ratio decreases. It indicates that the UHPFRCFST columns can efficiently be adopted to improve the bending capacity with the small diameter-to-thickness ratio. Furthermore, a *D*/*t* ratio less than 25.60 should be maintained to ensure the required ductility of a CFST column made of UHPFRC, which also prevents the long steel tube from the local buckling (Fig. 15).

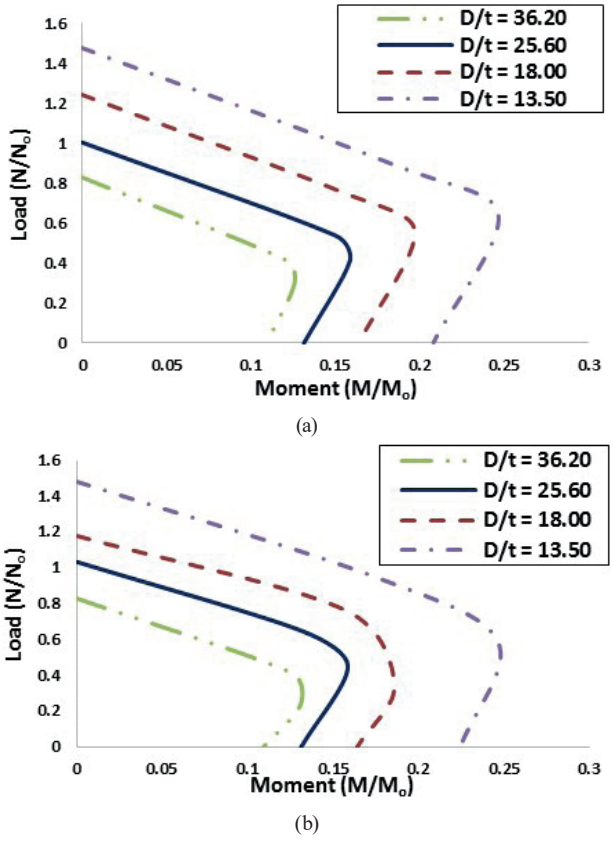

Fig. 14 *N*–*M* interaction diagram with various D/t ratio: (a) short columns; (b) long columns

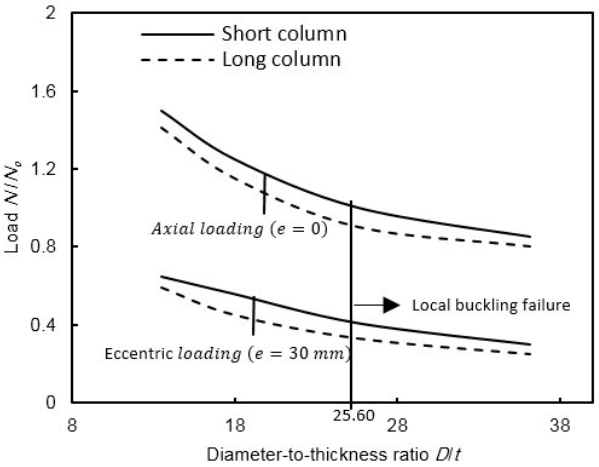

Fig. 15 Effect of *D*/*t* ratio on UHPFRCFST column strength

5 Interaction diagrams of the UHPFRCFSTs columns

The axial load-moment interaction curves (commonly termed N-M diagrams) from FE model, Eurocode 4 [40], GB 50936 [41], AIJ [42], AISC 360 [43], and experimental results are plotted in Fig. 16 for both short and long UHPFRCDSTs for thickness steel tube of 4 mm. The formulas used to predict the ultimate load capacity from four selected codes for the axial compression column CFST are shown in Table 4. The moment demands of the columns during were calculated as $M_u = N_u \times (e + \delta_m)$ where e is the initial eccentricity, and δ_m is the measured deflection, and N_u is the measured axial force.

Note, in Eurocode [40] N_1 is the characteristic plastic cross-sectional compressive resistance of a CFST without considering confinement for rectangular or square sections.

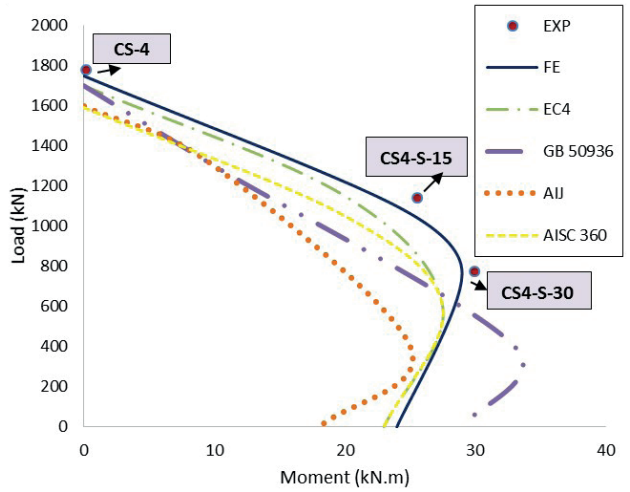

(a)

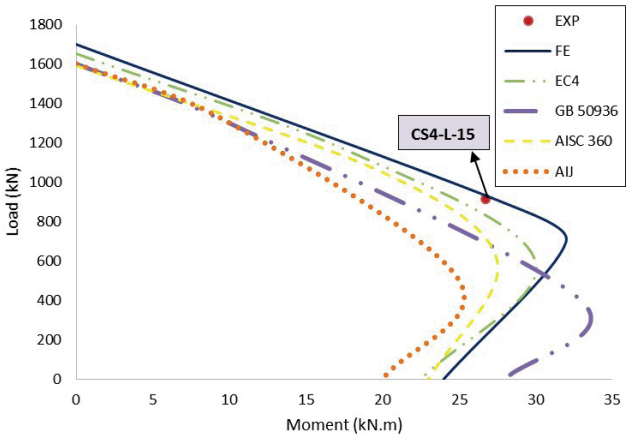

(b)

Fig. 16 Axial force –bending moment interaction diagram for UHPFRCFSTs columns: (a) short columns; (b) long columns

Table 4 Strength prediction methods for design codes

Codes	Expressions	Notes
Eurocode 4 [40]	$N_1 = A_s F_y + A_c F_{ck}$ $N_2 = \eta_s A_s F_y + A_c F_{ck}$ $(1 + \eta_c \frac{t}{D}\frac{Fy}{Fck})$, confinement effect (circular section)	$\eta_s = 0.25(3 + 2\lambda) +$ $(1 - 0.25(3 + 2\lambda))(10e/D)$ $\eta_c = (4.90 - 18.5\lambda + 17$ $\lambda^2)(1 - 10e/D)$
GB 50936 [41]	$N = A_{sc} F_{sc}$	$F_{sc} = (1.212 + B\theta + C\theta^2)$ F_c $\theta = \alpha_s \frac{F}{Fc}$, $\alpha = \frac{As}{Ac}$
AIJ guide [42]	$N = A_c F_{ck} + (1 + \eta) A_s F_y$	η = 0 square η = 0.27 circular
ANSI/AISC [43]	$N_2 = \eta_s A_s F_y + A_c F_{ck}$ $(1 + \eta_c \frac{t}{D}\frac{Fy}{Fck})$, confinement effect (circular section)	$P_p = F_y A_s + C_2 F_{ck} A_c$ $C_2 = 0.85$ rectangular $C_2 = 0.95$ circular
	Non-compact $N = P_p - \frac{P_p - P_y}{(\lambda_r - \lambda_y)^2}(\lambda - \lambda_p)^2$	$P_y = F_y A_s + 0.7 F_{ck} A_c$ $\lambda, \lambda_p, \lambda_r$: section slenderness ratios

Confinement effect may be considered for circular CFST with non-dimensional slenderness ratio ($\lambda \leq 0.50$) and the ratio of load eccentricity to diameter ($e/D < 0.5$), where λ is the non-dimensional slenderness ratio = $\sqrt{\frac{N1}{Ncr}}$, N_{cr} is the Euler buckling force of the CFST. t, D is the thickness and the diameter of steel tube. The Euler buckling force N_{cr} is formulated as:

$$N_{cr} = \frac{\pi^2 (EI)_{eff}}{l^2}, \tag{18}$$

$$EI_{eff} = E_s I_s + 0.60 E_c I_c, \tag{19}$$

where,

L is column length; E_c and E_s are the modulus of elasticity of concrete and steel; I_s and I_c are the second moment of area of steel and concrete sections, respectively. In GB50396 [41], θ means the hoop coefficient of concrete-filled steel tubular members, α_{sc} represents the steel content of concrete-filled steel tubular members, in the design of compressive strength of concrete-filled steel tube, B and C are the influence factors of the cross-sectional shape on the hoop effect, and about circular cross section.

It can be seen from the FE model and the experimental results in Fig. 16 that the proposed FE model results have acceptable high results. It can be seen that for short columns, GB 50936 and AISC 360 give relatively large predictions with N_{code}/N_{FE} of 1.12 and 1.01, respectively, while EC4 and AIJ are conservative in their predictions, with N_{code}/N_{FE} of 0.98 and 0.94. For long columns under pure axial loading, all codes give conservative predictions, with N_{code}/N_{FE} of 0.95, 0.97, 0.99 and 0.93, respectively. The N-M interaction diagram curve recommended by EC4 provides conservative results compared with both experimental and FE results.

6 Conclusions

In this paper, FE model was developed to investigate the behaviors of UHPFRCFSTs under axial or eccentric loading conditions. The novelty of this model is taken into account the confinement behavior of UHPFRC in the FE model. Using a validated FE model, three parametric studies are carried out. The following conclusions can be made:

1. It was shown that the FE models developed for the UHPFRCFSTs can predict accurately the ultimate capacities, load-mid height lateral displacement relationship, and interaction diagram curves. This indicates that the currently suggested FE model provides an accurate tool for representing the performance of UHPFRCFSTs.

2. The FE simulations and test results achieved satisfactory agreement in terms of failure modes. The overall failure mode of both short and long UHPFRCFSTs under eccentric loading are in-plane bending. Local buckling and fracture of the steel tube are usually located in the middle-section of the columns.
3. The UHPFRC in a CFST column is found to be more efficient when it is subjected to pure axial loading as well as small eccentricity. In contrast to the effect of UHPFRC, the pure bending capacity increases as the steel yield strength increases.
4. Based on the results of the current study, a diameter-to-thickness ratio should not be greater than 25.60 to prevent the steel tube from the local buckling.
5. AISC 360 code displays the greatest accuracy in predicting load bearing capacity, with average N_{code}/N_{FE} values of 1.01 and 0.97 for short and long columns, respectively. The most conservative projections were provided by AIJ, followed by EC4, AISC 360, and GB 50936. By comparing the FE curve with the *N–M* interaction curve calculated by the design code, EC4 expected the best results, but still needed more improvement.

Acknowledgement

The authors declare that they have no known competing financial interests or personal relationships that could have appeared to influence the work reported in this paper.

References

[1] Shanmugam, N. E., Lakshmi, B. "State of the art report on steel concrete composite columns", Journal of Constructional Steel Research, 57(10), pp. 1041–1080, 2001. https://doi.org/10.1016/S0143-974X(01)00021-9

[2] Han, L.-H., Li, W., Bjorhovde, R. "Developments and advanced applications of concrete-filled steel tubular (CFST) structures: Members", Journal of Constructional Steel Research, 100, pp. 211–228, 2014. https://doi.org/10.1016/j.jcsr.2014.04.016

[3] Ahmadi, M., Naderpour, H., Kheyroddin, A., Gandomi, A. H. "Seismic Failure Probability and Vulnerability Assessment of Steel-Concrete Composite Structures", Periodica Polytechnica Civil Engineering, 61(4), pp. 939–950, 2017. https://doi.org/10.3311/PPci.10548

[4] Martinavičius, D., Augonis, M., Arruda, M. R. T. "Experimental and Analytical Study on Local Buckling Behavior of the Concrete-filled Thin-walled Welded Steel Columns", Periodica Polytechnica Civil Engineering, 64(3), pp. 917–927, 2020. https://doi.org/10.3311/PPci.15705

[5] Labibzadeh, M., Jamalpour, R., Jing, D. H., Khajehdezfuly, A. "A Numerical Comparison between Spiral Transverse RC and CFST Columns under Loads of Varying Eccentricities", Periodica Polytechnica Civil Engineering, 63(4), pp. 1171–1182, 2019. https://doi.org/10.3311/PPci.14177

[6] Lee, S.-H., Uy, B., Kim, S.-H., Choi, Y.-H., Choi, S.-M. "Behavior of high-strength circular concrete-filled steel tubular (CFST) column under eccentric loading", Journal of Constructional Steel Research, 67(1), pp. 1–13, 2011. https://doi.org/10.1016/j.jcsr.2010.07.003

[7] Tokgoz, S., Dundar, C. "Experimental study on steel tubular columns in-filled with plain and steel fiber reinforced concrete", Thin-Walled Structures, 48(6), pp. 414–422, 2010. https://doi.org/10.1016/j.tws.2010.01.009

[8] Lu, Y., Li, N., Li, S., Liang, H. "Behavior of steel fiber reinforced concrete-filled steel tube columns under axial compression", Construction Building Material, 95(10), pp. 74–85, 2015. https://doi.org/10.1016/j.conbuildmat.2015.07.114

[9] Ghazy, M. F., Abd Elaty, M. A., Zalhaf, N. M. "Mechanical Properties of HPC Incorporating Fly Ash and Ground Granulated Blast Furnace Slag After Exposure to High Temperatures", Periodica Polytechnica Civil Engineering, 66(3), pp. 761–774, 2022. https://doi.org/10.3311/PPci.19751

[10] Kizilkanat, A. B. "Experimental Evaluation of Mechanical Properties and Fracture Behavior of Carbon Fiber Reinforced High Strength Concrete", Periodica Polytechnica Civil Engineering, 60(2), pp. 289–296, 2016. https://doi.org/10.3311/PPci.8509

[11] Aydın, S. "Effects of fiber strength on fracture characteristics of normal and high strength concrete", Periodica Polytechnica Civil Engineering, 57(2), pp. 191–200, 2013. https://doi.org/10.3311/PPci.7174

[12] Paschalis, S., Lampropoulos, A. "Fiber content and curing time effect on the tensile characteristics of ultra-high performance fiber reinforced concrete", Structural Concrete, 18(4), pp. 577–588, 2017. https://doi.org/10.1002/suco.201600075

[13] Qi, J., Cheng, Z., Wang, J., Tang, Y. "Flexural behavior of steel-UHPFRC composite beams under negative moment", Structures, 24, pp. 640–649, 2020. https://doi.org/10.1016/j.istruc.2020.01.022

[14] Hashim, D. T., Hejazi, F., Jaafar, M. S., Lai, V. Y. "The Performance Evaluation of Circular Flange Bolted Connection in Ultra High Performance Fiber Reinforced Concrete Segmented Communication Tower", Periodica Polytechnica Civil Engineering, 63(4), pp. 971–988, 2019. https://doi.org/10.3311/PPci.12697

[15] Sakr, M. A., Osama, B., El Korany, T. M. "Modeling of ultra-high performance fiber reinforced concrete columns under eccentric loading", Structures, 32, pp. 2195–2210, 2021. https://doi.org/10.1016/j.istruc.2021.04.026

[16] Sakr, M. A., El Korany, T. M., Osama, B. "Analysis of RC columns strengthened with ultra-high performance fiber reinforced concrete jackets under eccentric loading", Engineering Structures, 220, 111016, 2020. https://doi.org/10.1016/j.engstruct.2020.111016

[17] Sakr M. A., Saad, A. G., El-korany, T. M. "Analysis of exterior beam-column joints under varying column axial load and code comparisons", Advances in Structural Engineering, 25(4), pp. 837–863, 2022.
https://doi.org/10.1177%2F13694332211050979

[18] Eladly, M. M. "Numerical study on masonry-infilled steel frames under vertical and cyclic horizontal loads", Journal of Constructional Steel Research, 138, pp. 308–323, 2017.
https://doi.org/10.1016/j.jcsr.2017.07.016

[19] Mursi, M., Uy, B. "Strength of concrete filled steel box columns incorporating interaction buckling", Journal of Structural Engineering, 129(5), pp. 626–639, 2003.
https://doi.org/10.1061/(ASCE)0733-9445(2003)129:5(626)

[20] Mursi, M., Uy, B. "Strength of slender concrete filled high strength steel box columns", Journal of Constructional Steel Research, 60(12), pp. 1825–1848, 2004.
https://doi.org/10.1016/j.jcsr.2004.05.002

[21] Sakino, K., Nakahara, H., Morino, S., Nishiyama, I. "Behavior of centrally loaded concrete-filled steel-tube short columns", Journal of Structural Engineering, 130(2), pp. 180–188, 2004.
https://doi.org/10.1061/(ASCE)0733-9445(2004)130:2(180)

[22] Huang, Z., Li, D., Uy, B., Thai, H.-T., Hou, C. "Local and post-local buckling of fabricated high-strength steel and composite columns", Journal of Constructional Steel Research, 154, pp. 235–249, 2019.
https://doi.org/10.1016/j.jcsr.2018.12.004

[23] Zhang, T., Ding, F., Liu, X., Yu, Z. "Compressive behavior of steel-reinforced concrete-filled circular steel tubular stub columns", Structures, 28, pp. 863–877, 2020.
https://doi.org/10.1016/j.istruc.2020.08.012

[24] Ding, F., Luo, L., Zhu, J., Wang, L., Yu, Z. "Mechanical behavior of stirrup confined rectangular CFT stub columns under axial compression", Thin-Walled Structures, 124, pp. 136–150, 2018.
https://doi.org/10.1016/j.tws.2017.12.007

[25] Xiong, M.-X., Xiong, D.-X., Liew, J. Y. R. "Axial performance of short concrete filled steel tubes with high- and ultra-high- strength materials", Engineering Structures, 136(4), pp. 494–510, 2017.
https://doi.org/10.1016/j.engstruct.2017.01.037

[26] Chen, S. Zhang, R., Jia, L.-J., Wang, J.-Y., Gu, P. "Structural behavior of UHPC filled steel tube columns under axial loading", Thin-Walled Structures, 130, pp. 550–563, 2018.
https://doi.org/10.1016/j.tws.2018.06.016

[27] Zhang, R., Chen, S., Gu, P., Huang, Y. "Structural behavior of UHPC filled steel tubular columns under eccentric loading", Thin-Walled Structures, 156, 106959, 2020.
https://doi.org/10.1016/j.tws.2020.106959

[28] Yan, Y., Xu, L., Li, B., Chi, Y., Yu, M., Zhou, K., Song, Y. "Axial behavior of ultra-high performance concrete (UHPC) filled stocky steel tubes with square sections", Journal of Constructional Steel Research, 158, pp. 417–428, 2019.
https://doi.org/10.1016/j.jcsr.2019.03.018

[29] Hoang, A. L., Fehling, E., Lai, B., Thai, D.-K., Chau, N. V. "Experimental study on structural performance of UHPC and UHPFRC columns confined with steel tube", Engineering Structures, 187, pp. 457–477, 2019.
https://doi.org/10.1016/j.engstruct.2019.02.063

[30] Yang, Y., Wu, C., Liu, Z., Qin, Y., Wang, W. "Comparative study on square and rectangular UHPFRC-Filled steel tubular (CFST) columns under axial compression", Structures, 34, pp. 2054–2068, 2021.
https://doi.org/10.1016/j.istruc.2021.08.104

[31] Hassanein, M. F., Patel, V. I. "Round-ended rectangular concrete-filled steel tubular short columns: FE investigation under axial compression", Journal of Construction Steel Research, 140, pp. 222–236, 2018.
https://doi.org/10.1016/j.jcsr.2017.10.030

[32] Ouyang, Y., Kwan, A. K. H. "Finite element analysis of square concrete-filled steel tube (CFST) columns under axial compressive load", Engineering Structures, 156, pp. 443–459, 2017.
https://doi.org/10.1016/j.engstruct.2017.11.055

[33] dos Santos, L. R., de Sousa Cardoso, H., Caldas, R. B., Figueiredo Grilo, L. "Finite element model for bolted shear connectors in concrete-filled steel tubular columns", Engineering Structures, 203, 109863, 2020.
https://doi.org/10.1016/j.engstruct.2019.109863

[34] ABAQUS "Analysis User's Manual, Version 6.14", [software] Available at: https://www.3ds.com

[35] Naeimi, N., Moustafa, M. A. "Analytical stress–strain model for steel spirals-confined UHPC", Composites Part C: Open Access, 5, 100130, 2021.
https://doi.org/10.1016/j.jcomc.2021.100130

[36] Wille, K., El-Tawil, S., Naaman, A. E. "Properties of strain hardening ultra-high performance fiber reinforced concrete (UHP- FRC) under direct tensile loading", Cement Concrete Composites, 48, pp. 53–66, 2014.
https://doi.org/10.1016/j.cemconcomp.2013.12.015

[37] AFGC/SETRA "Interim recommendations on Ultra High Performance Fibre-Reinforced Concretes (UHPC)", AFGC Scientific and Technical Documents, Canberra, Australia, 2013.

[38] Tao, Z., Wang, Z.-B., Yu, Q. "Finite element modelling of concrete-filled steel stub columns under axial compression", Journal Constructional Steel Research, 89(5), pp. 121–131, 2013.
https://doi.org/10.1016/j.jcsr.2013.07.001

[39] Singh, M., Mohamed Ali, M. S., Sheikh, A. H., Griffith, M., Visintin, P. "Structural behavior of ultra-high performance fiber reinforced concrete beams with steel and polymer bar reinforcement", In: Proceedings of The 11th fib International PhD Symposium in Civil Engineering, Tokyo, Japan, 2016, pp. 287–294.

[40] CEN "Eurocode 4, Design of Composite Steel and Concrete Structures. Part 1-1: General Rules and Rules for Building (EN 1994-1-1:2004)", European Committee for Standardization, Brussels, Belgium, 2004.

[41] JSA "GB 50936-2014, Technical Code for Concrete Filled Steel Tubular Structures", China Architecture & Building Press, Beijing, China, 2014. (in Chinese)

[42] AIJ "Recommendations for Design and Construction of Concrete Filled Steel Tubular Structures", Architectural Institute of Japan, Tokyo, Japan, 2008. (in Japanese)

[43] AISC "ANSI/AISC 360-10, Code for Structural Steel Buildings", American Institute of Steel Construction, Chicago, IL, USA, 2010.